AIAA JOURNAL
Vol. 46, No. 1, January 2008

Dynamic Compensation of a Synthetic Jetlike Actuator for Closed-Loop Cavity Flow Control

Kihwan Kim,* Marco Debiasi,† Ryan Schultz,‡ Andrea Serrani,§ and Mo Samimy¶
The Ohio State University, Columbus, Ohio 43210

DOI: 10.2514/1.30095

Actuation devices are crucial components of closed-loop flow control schemes. Synthetic jetlike actuators, which are commonly employed in cavity flow control, exhibit a dynamic response that, if ignored, may significantly affect the overall characteristics of the closed-loop system. This paper presents the development and implementation of a dynamic compensator for a synthetic jetlike compression driver actuator which has been successfully implemented for feedback control of subsonic cavity flows. A time-delay model of the actuator dynamics is obtained from experimental data using subspace-based identification methods. The model is designed to match the frequency response of the physical system in a frequency range of interest that covers the resonance frequencies of the cavity. The model is then used for the synthesis of a dynamic controller which employs a Smith predictor in conjunction with an H_∞ mixed-sensitivity design. Order reduction is applied to obtain a low-order digital controller amenable to real-time applications. The compensator is retrofitted to an existing cavity flow control architecture, and used to force the actuator output to closely follow the input commands, thereby compensating undesirable actuator dynamics. Experiments show that the integration of the actuator compensator within the cavity control system significantly improves closed-loop performance.

I. Introduction

SUPPRESSION of pressure oscillations induced by a flow over a shallow cavity—a configuration occurring in many practical applications, from landing gear wells to weapon bays—is a recognized benchmark problem in active flow control [1–3]. The flow over a shallow cavity produces self-sustained oscillations caused by coupling between flow dynamics and flow-generated acoustic field [3], leading to pressure fluctuations that can be very intense. For the development of active cavity flow control strategies, although feedforward schemes have been attempted with various degrees of success [4,5], in recent years the most significant effort has been spent on feedback control (see [6,7] for a comprehensive review).

The flow control group within the Collaborative Center of Control Science at The Ohio State University has developed and tested several methodologies for feedback control of subsonic cavity flows. Specifically, for the physically based linear model proposed by Rowley et al. [8], it has been shown in [9] that proportional and delay-based controllers are capable of reducing the dominant resonance for which they are designed, but may introduce tones at other frequencies. Although a subsequent approach based on neural networks has showed some potential [10], significant results have been accomplished by developing linear-quadratic controllers on the basis of reduced-order flow models [11–13]. In all the above mentioned studies, a compression driver acoustic actuator has been employed within the feedback control architecture to excite the flow at the leading edge of the cavity. This actuator, capable of producing zero-net-mass flow in a wide frequency band, has enough authority to significantly alter the flow at subsonic speed. To date, the actuator has been treated as a constant-gain element that produces an output proportional to a control signal. This assumption could have negative effects on the overall flow control system when the device's own dynamics cannot be neglected. This is indeed the case for the actuator implemented in our studies, which exhibits a distinct frequency-dependent behavior caused by the geometric features of the converging nozzle channeling the actuator output to the leading edge of the cavity. In particular, it has been experimentally verified that

1) A significant time delay exists between the input (voltage) and output signals (pressure or flow velocity), due to the propagation time of acoustic waves from the compression driver to the actuator exit slot. Time delay is known to severely limit the bandwidth of a feedback control system [14].

2) The actuator output shows distinct resonance peaks in the frequency domain due to the infinite-dimensional characteristics of the system [5] stemming from acoustics-related reflection and transport delay. This implies that there may be significant distortion between the actuator input and the actuated output signals.

The objective of this paper is to develop a methodology for feedback compensation of the dynamics of synthetic jetlike actuators, to be employed in closed-loop flow control schemes. To this end, the design of a model-based feedback controller for the specific actuator device used in [11–13], and its incorporation in the existing control architecture, will be presented as a representative case study for these types of application.

In the literature, analytical and physics-based models of synthetic jet actuators have been proposed using the unsteady Bernoulli equation coupled with structural modeling [15,16], lumped element modeling [17], and transfer function methods with mechanical elements [18]. In the cited references, the geometric dimensions of the actuators were smaller than the characteristic wavelength, so that it was possible to neglect internal acoustic phenomenon [17]. This assumption is inappropriate for the compression-driver-type actuator which is the object of our investigation, because the nozzle length is comparable to the sound wavelength [5]. As for acoustic ducts with speakers, whose structures are analogous to the compression driver actuator, analytical models can be derived from the wave equation

Presented as Paper 880 at the 45th AIAA Aerospace Sciences Meeting and Exhibit, Reno, Nevada, 8–11 January 2007; received 29 January 2007; revision received 28 June 2007; accepted for publication 30 August 2007.

*Post Doctoral Researcher, Collaborative Center of Control Science, Department of Electrical and Computer Engineering. Member AIAA.

†Research Scientist, Collaborative Center of Control Science, Department of Mechanical Engineering; currently at Temasek Laboratories, National University of Singapore. Member AIAA.

‡Graduate Student, Collaborative Center of Control Science, Department of Electrical and Computer Engineering.

§Assistant Professor, Collaborative Center of Control Science, Department of Electrical and Computer Engineering. Member AIAA.

¶Professor and Director, Collaborative Center of Control Science, Gas Dynamics and Turbulence Laboratory, Department of Mechanical Engineering. Associate Fellow AIAA.

that describes the acoustic dynamics [19,20]. In particular, for the actuators with converging nozzles, Webster's horn equation can be used to derive the governing equations [21]. However, from a control-oriented perspective, this approach will yield a poor model for the actuator used in this research, because it is difficult to determine the boundary condition accounting for the interaction with cavity flow at the actuator exit slot [22]. Furthermore, the geometric shape of the nozzle is specially designed [5] so that its shape cannot be readily incorporated into the model equation [22].

In this research, a black-box model approach using experimental input–output data sets is considered as an alternative method to derive a control-oriented model of the actuator dynamics. McKelvey et al. [23] showed that subspace-based system identification using frequency-domain data can be an effective tool to identify highly resonant dynamics that occur frequently in acoustic systems. This approach is pursued in our study, where subspace-based system identification using frequency-domain data is implemented to construct a linear time-invariant model of the actuator to capture the relevant dynamics in the frequency range of interest, while being of sufficiently low order to be feasible for real-time application. In addition, the presence of time delay, experimentally determined from the step response, can be taken explicitly into account in the model structure.

An actuator compensator, designed on the basis of the identified model, aims at increasing the open-loop gain and alleviating the unfavorable frequency peaks in the actuator outputs. For the closely related problem of noise cancellation inside acoustic ducts, control approaches employing adaptive, fuzzy-logic, linear-quadratic-Gaussian (LQG), or H_∞ optimization schemes have been explored [20,24–28]. Feedback control design for acoustic applications needs more careful consideration than the conventional feedback control applications, as the frequency response of these systems does not roll off at high frequency and shows strong resonance peaks [20]. As a result, feedback controllers based on linear finite-dimensional models must ensure robust stability to deal with uncertainties caused by discrepancies between the model and the physical system. For this study, a Smith-predictor-type control structure is employed to account for the time delay [29], while an H_∞ mixed-sensitivity method is adopted for control synthesis as an effective means to provide robustness against unmodeled dynamics. Bounds on model uncertainties can be assessed quantitatively in the frequency domain, in terms of H_∞ norm of appropriate weighting functions that are employed in the controller design [14].

The effect of the integration of the actuator compensator on an existing feedback cavity flow control system is then examined experimentally. Results show that the compensator forces the actuator output to follow closely the reference command in the frequency range of interest, thereby suppressing spurious peaks in sound pressure spectra previously measured in closed-loop operations. As a result, the performance of the original cavity flow controller can be more clearly assessed from experimental data. In addition, experiments performed in off-design conditions show that the compensator extends the range of Mach numbers of the freestream flow in which the controller is effective.

The paper is organized as follows: In Sec. II, the experimental setup adopted to investigate the actuator characteristics and to collect data used for identification and model validation is introduced. In Sec. III, the subspace-based system identification method is discussed, and the fidelity of the model is assessed in comparison with experimental data. Section IV presents the Smith predictor/H_∞ approach to the design of the actuator servocontroller. The integration of actuator compensation within the existing cavity flow control system is described in Sec. V, where experimental results are discussed. Concluding remarks are given in Sec. VI.

II. Experimental Setup and Data Acquisition

The experimental facility used in this study, shown in Fig. 1, is an optically accessible small scale blow-down wind tunnel located at the Gas Dynamics and Turbulence Laboratory of The Ohio State University. The tunnel can operate in the subsonic range between Mach 0.20 and Mach 0.70. Flow is directed to the 50.8 mm × 50.8 mm test section through a converging nozzle before exhausting to the atmosphere. A shallow cavity is recessed in the test section with a depth $D = 12.7$ mm and length $L = 50.8$ mm for a length to depth aspect ratio L/D equal to 4. The actuator consists of a Selenium D3300Ti compression driver connected to a 108-mm-long nozzle that converges from the driver to an exit slot of width 1 mm. The diaphragm movement of the compression driver creates oscillatory flow that exits through the slot at an angle of 30 deg with respect to the freestream flow in the tunnel. Further details on the setup can be found in [5].

For a voltage signal V_a applied to the compression driver, three output variables are measured simultaneously, namely, pressures p_i and p_o inside and outside the nozzle, respectively, and flow velocity v_j exiting the nozzle (see Fig. 1). The pressure fluctuations are measured by flush-mounted Kulite XCS-062-30A and XCL-100-25A transducers, respectively. The velocity v_j is acquired using a TSI 1276-10A subminiature hot-film probe. The signals pass through an antialiasing filter with a 10 kHz cutoff frequency. A dSpace 1103 DSP board operating at 50 kHz sampling rate is used to manage the data acquisition and the implementation of the feedback control algorithms.

The characteristics of the experimental setup have been thoroughly investigated in previous work [5,13]. At Mach 0.3, the cavity flow shows a time-invariant, single-mode resonance corresponding to the third Rossiter mode. For this condition, it has been verified that the actuator has sufficient control authority to alter the behavior of the flow. Therefore, the flow at Mach 0.3 is chosen as a reference baseline for this research. In what follows, the relationship between the input voltage and the measured output variables are examined, using random noise inputs varied from 1 to 5 V in terms of rms magnitude. As shown in Fig. 2, all output variables show a linear relationship with the input in the absence of flow in the tunnel, whereas they are affected by the addition of the flow at Mach 0.3. However, the inside pressure shows a relatively smaller sensitivity to freestream conditions compared to the other two variables, because it is measured at a location shielded from the effects of the external flow. Figure 3 shows the frequency response of each output variable obtained using a random noise voltage input with rms magnitude equal to 5 V. Evidently, the frequency response of the inside pressure is almost independent of main flow, whereas the characteristics of two other variables change significantly with the Mach number. These results are in accordance with the results in Fig. 2. Numerous resonance peaks are observed in all three responses, believed to originate from the infinite-dimensional nature of the actuator dynamics. The differences between the peaks and the valleys are of order 10–20 dB for pressures and 30 dB for velocity. Finally, Fig. 4 shows the spectra of the inside and outside pressures at the actuator exit when $V_a = 0$ at baseline Mach 0.30 flow. It can be seen that while both p_i and p_o oscillate at about 2.85 kHz (the resonance frequency of the baseline cavity flow), only the inside pressure p_i exhibits high-frequency peaks. This confirms that the peaks of the frequency response in Fig. 3 are not related to the acoustics of the cavity, but to the internal dynamics of the actuator. It

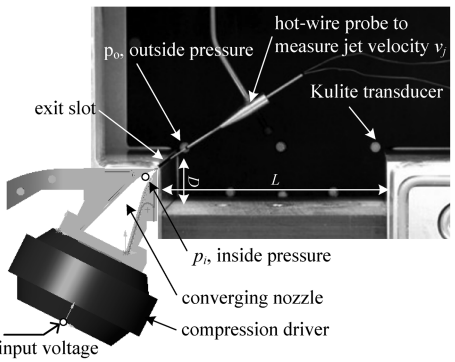

Fig. 1 Schematic of experimental setup showing the cavity model and the actuator.

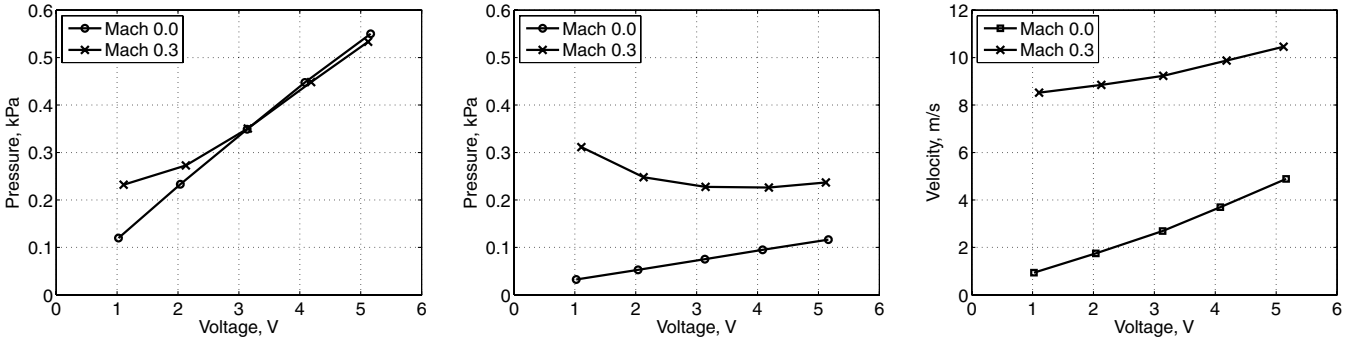

a) Inside pressure p_i **b) Outside pressure p_o** **c) Actuator output velocity v_j**

Fig. 2 Relationships between the output flow variables and the input voltage in terms of rms magnitude with and without main flow.

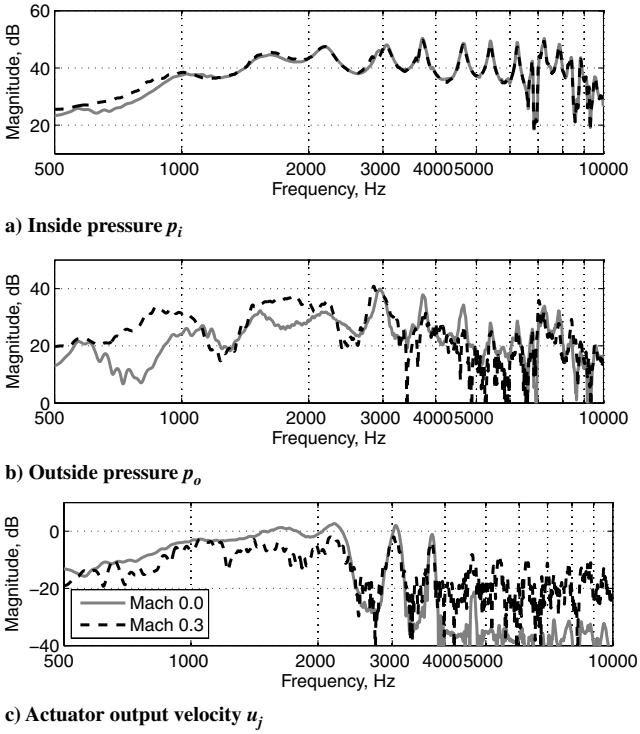

a) Inside pressure p_i

b) Outside pressure p_o

c) Actuator output velocity u_j

Fig. 3 Frequency responses of the measured variables with and without main flow.

is apparent that, if the actuator dynamics is not compensated, the amplitude of the actuator output would be severely distorted when operating in the considered frequency range.

Based on this analysis, the inside pressure p_i is selected as the output variable of the actuator model. The inside pressure exhibits

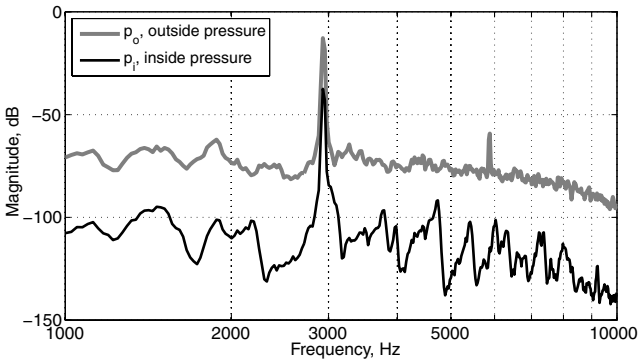

Fig. 4 Frequency spectra of inside and outside pressure fluctuations for the baseline flow (Mach 0.30).

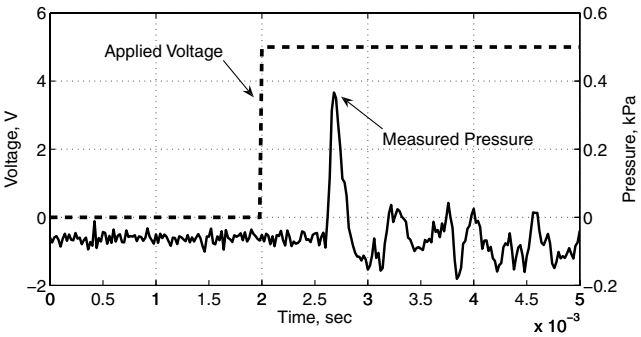

Fig. 5 Response of the inside pressure p_i with respect to a step input.

the most consistent linear input–output relationship among the measured variables irrespective of tunnel flow, while its frequency response represents well the common characteristics of all the output variables. Furthermore, surface pressure fluctuations can be easily measured in real time using flush-mounted transducers without disrupting cavity flow, compared to the measurement of velocity fluctuations with a hot-wire probe.

The time delay between the input voltage and the inside pressure can be estimated from the output response with respect to a step input. As shown in Fig. 5, the time difference between the rising edges of the input and output signals is estimated to be equal to 0.62 ms. This value is adopted as the time delay τ for the system identification.

III. Subspace-Based System Identification

The linear actuator model in the state-space representation is selected as

$$\begin{aligned} \dot{x}(t) &= Ax(t) + Bu(t-\tau) \\ y(t) &= Cx(t) + Du(t-\tau) + \delta(t) \end{aligned} \tag{1}$$

where $u(t) \in \mathbb{R}$ is the input, $y(t) \in \mathbb{R}$ the output, $x(t) \in \mathbb{R}^{n\times 1}$ the state, and $\delta(t) \in \mathbb{R}$ the measurement noise, assumed Gaussian. The system matrices are denoted by $A \in \mathbb{R}^{n\times n}$, $B \in \mathbb{R}^{n\times 1}$, $C \in \mathbb{R}^{1\times n}$, and $D \in \mathbb{R}$. The input $u(t)$ corresponds to the voltage signal $V_a(t)$ and the output variable to the inside pressure $p_i(t)$. The propagation time of the acoustic waves has been incorporated into the model structure as an input time delay τ. Applying Laplace transform to Eq. (1) yields

$$Y(s) = G(s)U(s) + \Delta(s) = e^{-\tau s}G_o(s)U(s) + \Delta(s) \tag{2}$$

where $G(s)$ is the model transfer function and $G_o(s) = C(sI - A)^{-1}B + D$ is its delay-free part. Provided that τ is known, estimates $(\hat{A}, \hat{B}, \hat{C}, \hat{D})$ of the system matrices (A, B, C, D) can be obtained by optimizing the following least-squares condition at discrete frequencies ω_k

$$\hat{G}_o(s) = \arg\min_{G_o(s)} \sum_{k=0}^{N-1} \|G(j\omega_k) - G_o(j\omega_k)e^{-\tau j\omega_k}\|^2$$
$$\omega_k = k\frac{\pi f_s}{N} \tag{3}$$

where $\hat{G}_o(s) = \hat{C}(sI - \hat{A})^{-1}\hat{B} + \hat{D}$. The constants f_s and N denote the sampling frequency and the number of data in the frequency domain, respectively. Assuming that the system is excited by a periodic signal band limited below the Nyquist frequency, the continuous-time transfer function $G(s)$ can be approximated with the discrete Fourier transform of the sampled input–output data set $(\tilde{U}(\omega_k), \tilde{Y}(\omega_k))$ as follows [30]:

$$G(j\omega_k) \approx \frac{\tilde{Y}(\omega_k)}{\tilde{U}(\omega_k)} \tag{4}$$

Using this condition, Eq. (3) is rewritten as

$$\hat{G}_o(s) = \arg\min_{G_o(s)} \left\| \sum_{k=0}^{N-1} \frac{\tilde{Y}(\omega_k)}{\tilde{U}(\omega_k)} - G_o(j\omega_k)e^{-\tau j\omega_k} \right\|^2 \tag{5}$$

where $\tilde{Y}(\omega_k)/\tilde{U}(\omega_k)$ represents the empirical frequency response of the system. Because this empirical response tends to become noisier as the number of data N increases, a Hamming window function W_γ is employed to smooth it as follows [31]:

$$\bar{G}(j\omega_k) = \frac{\int_{-\pi}^{\pi} W_\gamma(\xi - \omega_k)|\tilde{U}(\xi)|^2[\tilde{Y}(\omega_k)/\tilde{U}(\omega_k)]\,\mathrm{d}\xi}{\int_{-\pi}^{\pi} W_\gamma(\xi - \omega)|\tilde{U}(\xi)|^2\,\mathrm{d}\xi} \tag{6}$$

where $\bar{G}(j\omega_k)$ stands for the empirical transfer function estimate (ETFE). Consequently, Eq. (5) is modified as

$$\hat{G}_o(s) = \arg\min_{G_o(s)} \sum_{k=0}^{N-1} \|\bar{G}(j\omega_k) - G_o(j\omega_k)e^{-\tau j\omega_k}\|^2 \tag{7}$$

This equation can be readily computed using the MATLAB routine N4SID [32]. In general, the state-space forms obtained from the subspace method lead to excessively high-order systems. Hence, model reduction of the identified system is required for the sake of designing a practical controller that can be implemented in real time. Balanced realization and truncation methods are employed to this end. Applying a balancing similarity transformation $x_b = Tx$ to the identified system matrices $(\hat{A}, \hat{B}, \hat{C}, \hat{D})$ leads to [14]

$$\hat{A}_b = T\hat{A}T^{-1} = \begin{bmatrix} \hat{A}_b(1,1) & \hat{A}_b(1,2) \\ \hat{A}_b(2,1) & \hat{A}_b(2,2) \end{bmatrix}$$
$$\hat{B}_b = T\hat{B} = \begin{bmatrix} \hat{B}_b(1,1) \\ \hat{B}_b(2,1) \end{bmatrix} \tag{8}$$
$$\hat{C}_b = \hat{C}T^{-1} = [\hat{C}_b(1,1)\ \ \hat{C}_b(1,2)], \qquad \hat{D}_b = \hat{D}$$

and yields the Gramian of $\hat{G}_o(s)$

$$\Sigma = \begin{bmatrix} \Sigma_1 & 0 \\ 0 & \Sigma_2 \end{bmatrix}$$

where $\Sigma_1 = \mathrm{diag}(\sigma_1, \ldots, \sigma_k)$ and $\Sigma_2 = \mathrm{diag}(\sigma_{k+1}, \ldots, \sigma_n)$ contain the ordered Hankel singular values of $\hat{G}_o(s)$, that is, $\sigma_1 > \cdots > \sigma_k > \sigma_{k+1} > \cdots > \sigma_n$. The value σ_i represents the relative contribution of the ith balanced state $x_{b,i}$ to the input–output relationship of the system. Consequently, the full-order system in n dimensions can be reduced to the kth-order system $(\hat{A}_b(1,1)\ \hat{B}_b(1,1)\ \hat{C}_b(1,1)\ \hat{D})$ by discarding the $n-k$ states associated with small Hankel singular values. Additional details of the balanced truncation method can be found in Antoulas [33].

The cavity flow controller operates in the frequency range of 1–5 kHz, which is adopted as a frequency range of interest [5,13]. For systems identification, chirp signals are designed to excite only the response of the actuator in the frequency range 400 Hz–9 kHz, while the rms magnitudes of the signals are kept larger than 4 V so as to minimize the effects of external flow conditions (refer to Fig. 2a). Four experimental data sets, obtained from chirp signals with different rms magnitudes, are merged into one set, and then filtered to contain only data in the range 600 Hz–6 kHz before being used for system identification. Recall that the infinite-dimensional actuator dynamics generate multiple resonance peaks over a wide frequency range, as seen in Fig. 3a. Conversely, the control-oriented model should be of a sufficiently low order to enable real-time application. Initially, the identification yielded a 22nd-order model, which was reduced to a 16th-order model by the balanced truncation method in Eq. (8). The transfer function of the resulting model is given by

Table 1 Poles and zeros of the transfer function $\hat{G}(s)$

i	$p_i(\times 10^4)$	$z_i(\times 10^4)$
0	——	-0.1534
1	$-0.0323 + 3.9402i$	$-0.1494 + 3.8576i$
2	$-0.0377 + 3.4089i$	$-0.1556 + 3.2652i$
3	$-0.0406 + 2.9340i$	$-0.1886 + 2.7234i$
4	$-0.0412 + 2.3508i$	$-0.1902 + 2.1487i$
5	$-0.0460 + 1.9212i$	$-0.3511 + 1.6866i$
6	$-0.0515 + 1.3680i$	$-0.2341 + 1.2995i$
7	$-0.0616 + 0.5856i$	$-0.1254 + 0.6681i$
8	$-0.0940 + 0.9876i$	——

$$\hat{G}(s) = e^{-\tau s} \cdot \frac{c(s - z_0)\prod_{i=1}^{7}(s - z_i)(s - \bar{z}_i)}{\prod_{i=1}^{8}(s - p_i)(s - \bar{p}_i)} \tag{9}$$

where $\tau = 0.00062$, $c = 791.3$, and $\bar{p}_i$ and $\bar{z}_i$ represent the complex conjugates of the poles p_i and zeros z_i, respectively, shown in Table 1. Note that the delay-free part in Eq. (9) is a stable and minimum phase system with relative-degree one. This model is used as a nominal plant for the controller synthesis. The frequency response of the model is shown in Fig. 6, together with the data set used in the procedure.

The modeling error can be assessed in the frequency domain in terms of the multiplicative model uncertainty [14]

$$L_I(\omega_k) = \max_{G_p \in \Pi} \left| \frac{G_p(j\omega_k) - \hat{G}_o(j\omega_k)e^{-\tau j\omega_k}}{\hat{G}_o(j\omega_k)e^{-\tau j\omega_k}} \right| \tag{10}$$

where Π stands for the set of all the possible responses of the system. In this study, the data set Π is computed collecting frequency response data acquired from several experiments using chirp input signals sweeping from 100 Hz to 15 kHz with various rms magnitude. The experimentally derived data set Π is then used to compute an estimate of the worst-case bound in Eq. (10). Note that the experimental data used for model validation are different from the data sets used for the identification. The uncertainty bound $L_I(\omega)$, shown in Fig. 7, remains below 30% for the frequency range 600 Hz–6 kHz, where the identification is performed, and increases substantially out of that range, as expected. It is worth noting that a

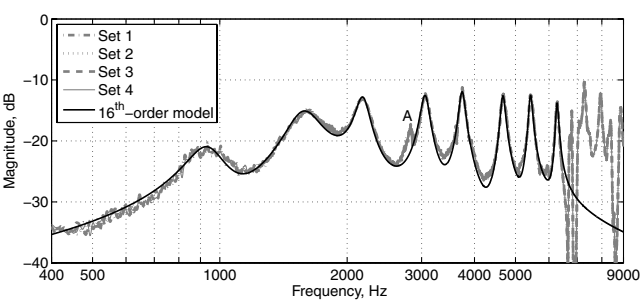

Fig. 6 Comparison between the frequency responses of the model and the data sets used for the identification. As for the experimental data sets 1–4, the input voltages are 6.00, 6.36, 6.72, and 7.00 V in terms of rms magnitude, respectively.

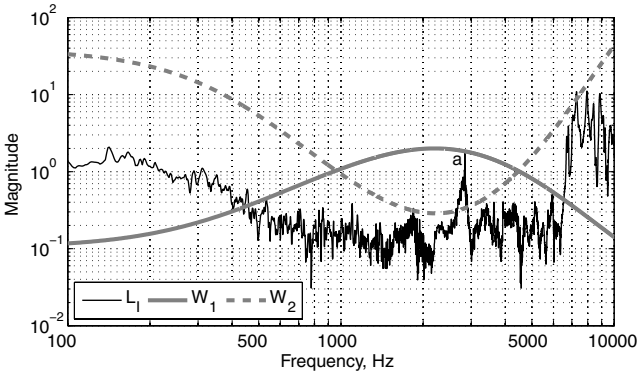

Fig. 7 Selection of weighting functions W_1 and W_2 based on the model uncertainty L_I.

sizable peak located at about 2.85 kHz (labeled a) is visible in the plot of the uncertainty bound in Fig. 7. This peak is not related to the actuator response; rather, it corresponds to the resonance peak of the cavity flow (compare with the peak labeled A in Fig. 6), which should not be captured by the system identification algorithm. Therefore, this frequency component is disregarded in the assessment of the model uncertainty of the actuator as far as the control synthesis is concerned. The multiplicative uncertainty bound thus obtained is employed in the following section for the selection of the complementary sensitivity weighting function for the H_∞ control synthesis.

IV. Compensator Design Based on H_∞ Control Synthesis

The aim of the compensator is to let the output of the model (9) track a time-varying reference signal $r(t)$ generated by a higher-level cavity flow controller. The presence of the time delay substantially complicates the design. Because the frequency response of a time-delay element $e^{-\tau s}$ is given by

$$|e^{-\tau \cdot j\omega}| = 1, \qquad \angle e^{-\tau \cdot j\omega} = -\tau\omega \tag{11}$$

the delay behaves as an all-pass filter with a linearly decreasing phase, thereby limiting the bandwidth and the achievable performance of the closed-loop system. Moreover, it is difficult to apply conventional control methods directly to time-delay systems, because $e^{-\tau s}$ is noninvertible and irrational [34]. To deal with the presence of time delay, a 2-degrees-of-freedom (2-DOF) controller incorporating a Smith predictor is adopted in this study. The structure of the controller is shown in Fig. 8. The complementary sensitivity function $T(s)$ of the closed-loop system, equivalent to the transfer function from the reference input r to the regulated output y, is computed as

$$T(s) = \frac{y(s)}{r(s)} = \frac{G_p(s)K(s)}{1 + [(1 - e^{-\tau s})G_o(s) + G_p(s)]K(s)} K_{\text{pre}}(s) \tag{12}$$

where $G_p(s)$ denotes the transfer function of a plant, and $K(s)$ and $K_{\text{pre}}(s)$ the transfer functions of a feedback controller and a prefilter, respectively. Provided that $G_p(s) = e^{-\tau s}G_o(s)$, the time delay is

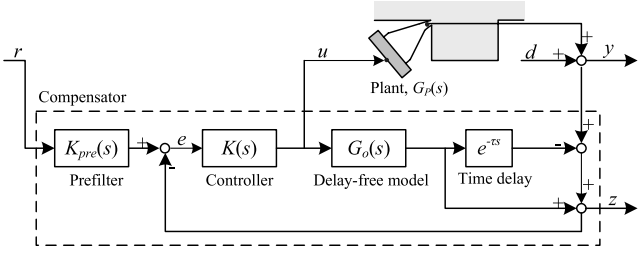

Fig. 8 Actuator compensator using 2 degree-of-freedom Smith-predictor-type control structure.

canceled out from the denominator of Eq. (12), as

$$T(s) = T_o(s)e^{-\tau s} \tag{13}$$

where

$$T_o(s) = \frac{G_o(s)K(s)}{1 + G_o(s)K(s)} K_{\text{pre}}(s)$$

is the pseudocomplementary sensitivity function $T_o(s)$, equivalent to the transfer function from the reference r to the pseudo-output z in Fig. 8. If $G_o(s)$ is stable and minimum phase, the controller $K(s)$ can be readily synthesized using standard loop-shaping techniques.

The compensated actuator output is expected to track the reference signal within the frequency interval $\Omega = \{\omega \mid \omega_l < \omega < \omega_h\}$ where the cavity flow controller operates. The lower and upper bounds ω_l and ω_h are determined from the frequency range of interest 1–5 kHz determined in Sec. III. The magnitude plot $|T(j\omega)|$ needs to be confined within a range of the form

$$1 - \delta_1 < |T(j\omega)| < 1 + \delta_2 \quad \text{for all } \omega \in \Omega \tag{14}$$

where δ_1 and δ_2 are determined by performance requirements. In addition, $|T(j\omega)|$ is required to exhibit sufficient roll-off for $\omega > \omega_h$ to maintain closed-loop stability in spite of model uncertainty.

As for any 2-DOF control structure, the feedback controller $K(s)$ plays a key role in reducing the system uncertainty, whereas a prefilter $K_{\text{pre}}(s)$ shapes the reference r to improve closed-loop performance. Ideally, it is best to synthesize the combined set $[K(s) \;\; K_{\text{pre}}(s)]$ in one step [35]. However, it is practical on occasion to determine $K_{\text{pre}}(s)$ based on the experimental responses of the closed loop where only the controller $K(s)$ is implemented, because the experimental results may differ from the analytical results [14]. The latter approach is pursued in this research. Assuming first that $K_{\text{pre}}(s) = 1$, an H_∞ mixed-sensitivity method is implemented for the synthesis of $K(s)$ [36,37]. The stabilizing $K(s)$ minimizes the H_∞ norm

$$\left\| \begin{bmatrix} W_1(s)S_o(s) \\ W_2(s)T_o(s) \end{bmatrix} \right\|_\infty \leqslant \gamma \tag{15}$$

where the function $S_o(s) = 1 - T_o(s)$ represents the sensitivity of the pseudo-output z with respect to the reference r. The weighting functions for $S_o(s)$ and $T_o(s)$ are denoted by $W_1(s)$ and $W_2(s)$, respectively. The conditions for nominal performance and robust stability of a closed loop are defined as [14]

$$\begin{aligned} &\text{nominal performance}: |W_1(j\omega)S_o(j\omega)| \leq 1, \quad \forall\ \omega \in \mathbb{R} \\ &\text{robust stability}: |W_2(j\omega)| \geq |L_I(j\omega)| \\ &|W_2(j\omega)T_o(j\omega)| \leq 1, \quad \forall\ \omega \in \mathbb{R} \end{aligned} \tag{16}$$

The H_∞ optimization problem in Eq. (15) can be numerically solved using the MATLAB routine hinfsyn. After this has been accomplished, the prefilter $K_{\text{pre}}(s)$ can be designed to satisfy

$$|K_{\text{pre}}(j\omega)| = |T_{\text{exp}}(j\omega)|^{-1}|T_{\text{ref}}(j\omega)|, \quad \forall\ \omega \in \mathbb{R} \tag{17}$$

where $T_{\text{exp}}(j\omega)$ is the frequency response of the closed-loop obtained from experimental data and $T_{\text{ref}}(j\omega)$ is the desired closed-loop response.

The crucial step in the H_∞ control synthesis is the choice of the weighting functions $W_1(s)$ and $W_2(s)$ satisfying the conditions in Eq. (16). Using the information on $L_I(\omega)$ obtained at the previous step, the weighting functions are selected as follows:

$$W_1(s) = \left\{ 35 \left[\frac{\tau_{11}s + r_{11}^{1/2}}{(\tau_{11}/r_{12}^{1/2})s + 1} \right]^2 \left[\frac{\tau_{12}s + r_{13}^{1/6}}{(\tau_{12}/r_{14}^{1/6})s + 1} \right]^6 \right\}^{-1} \tag{18}$$

$$W_2(s) = 80 \left[\frac{\tau_{21}s + r_{21}^{1/4}}{(\tau_{21}/r_{22}^{1/4})s + 1} \right]^4 \left[\frac{\tau_{22}s + r_{23}^{1/8}}{(\tau_{22}/r_{24}^{1/8})s + 1} \right]^8 \tag{19}$$

Table 2 Coefficients of the weighting functions $W_1(s)$ and $W_2(s)$

i	1	2	3	4
τ_{1i}	$(2\pi \cdot 1600)^{-1}$	$(2\pi \cdot 7500)^{-1}$	——	——
τ_{2i}	$(2\pi \cdot 1150)^{-1}$	$(2\pi \cdot 10000)^{-1}$	——	——
r_{1i}	55	0.03	0.005	100
r_{2i}	100	0.01	0.0048	10000

where the values of the coefficients are given in Table 2. The frequency response of the weighting functions is shown in Fig. 7 together with the uncertainty bound. As mentioned earlier, the weighting functions disregard the peak a, which is not related to the actuator dynamics. For the given selection of performance and robustness weights, the routine hinfsyn yields a 32nd-order feedback controller $K(s)$. This is then reduced to a 22nd-order controller $K_{\text{red}}(s)$ by means of the balanced truncation method in Eq. (8), and converted to a discrete controller $K_d(z)$ for real-time implementation at a 50 kHz sampling rate. Figure 9 confirms that the frequency response of the original controller below 10 kHz is preserved through this conversion.

The closed-loop response, shown in Fig. 10a, does not exhibit a sufficient gain and attenuation of the high-frequency components in absence of a prefilter. This is due to the fact that the robust stability condition in Eq. (16) limits the choice of $W_2(s)$, thus affecting the selection of the weighting factor $W_1(s)$ that determines the closed-loop performance. Following Eq. (17), a prefilter is designed using the inverse of the experimental closed-loop response as follows:

$$K_{\text{pre}}(s) = 1.25\left[\frac{\tau_1 s + r_1}{(\tau_1/r_2)s + 1}\right]\left[\frac{\tau_2 s + r_3^{1/2}}{(\tau_2/r_4^{1/2})s + 1}\right]^2 \tag{20}$$

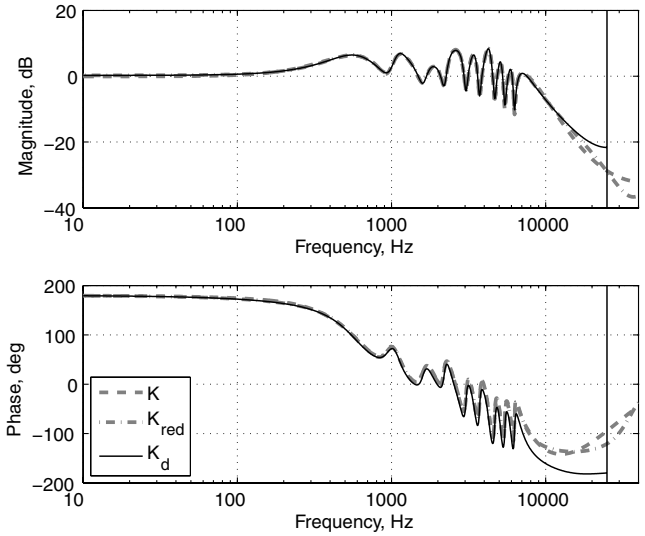

Fig. 9 Model reduction and discretization of a H_∞ feedback controller. K: a 32nd-order controller in the continuous time; K_{red}: a 22nd-order reduced controller; and K_d: a reduced-order controller in the discrete time.

where the values of the coefficients are $\tau_1 = (2\pi \cdot 740)^{-1}$, $\tau_2 = (2\pi \cdot 2700)^{-1}$, and $r_i (i = 1, \ldots, 4) = \{10, 0.095, 0.5, 100\}$. The addition of the prefilter noticeably improves the response of the compensated actuator dynamics, as seen from Figs. 10a and 10b, respectively. The response of the compensated actuator in Fig. 10b reveals that in the frequency range 1–5 kHz, the closed-loop gain is almost unitary and the fluctuation becomes smaller than ± 5 dB (compare with the uncompensated response in Fig. 6). Moreover, the response exhibits a favorable roll-off beyond 5 kHz, where the original dynamics show strong resonance peaks.

V. Implementation in Closed-Loop Cavity Flow Control

In this section, the integration of the actuator compensator with an existing cavity flow control architecture is discussed, and its effectiveness is evaluated experimentally. For the sake of completeness, the derivation of the controller is briefly summarized. The interested reader is referred to [11–13] for details.

A. Cavity Flow Control Architecture

The cavity flow controller employed in this study has been developed on the basis of a reduced-order flow model, obtained by means of proper orthogonal decomposition (POD) and Galerkin projection methods. For two-dimensional flows, the flowfield can be represented by the vector $\mathbf{q}(x, t) = [u(x, t)v(x, t)c(x, t)]$, where u and v are the velocity components, and c is the local speed of sound. The POD method approximates the flow variables in terms of finite-dimensional expansion

$$\mathbf{q}(\mathbf{x}, t) \cong \mathbf{q}_0(x) + \sum_{i=1}^{n} a_i(t)\varphi_i(\mathbf{x}) \tag{21}$$

where $\mathbf{q}_0(x)$ is the mean flow, and $\varphi_i(\mathbf{x})$ and $a_i(t)$ stand for the POD modes and the corresponding modal coefficient, respectively. For model development, 1000 particle image velocimetry (PIV) snapshots of the baseline flowfield were acquired to compute an expansion onto four POD modes. For linear control design, a linearized reduced-order model of the flowfield was derived applying the following steps:

1) Galerkin projection of the compressible Navier–Stokes equations onto the subspace spanned by the POD modes. This procedure yields a set of nonlinear ordinary differential equations (ODEs) governing the temporal evolution of $\mathbf{a}(t) = [a_1(t) \cdots a_n(t)]$.

2) Control separation using a spatial subdomain approach [38] to render explicit the presence of the control input Γ in the equations.

3) Linearization of the nonlinear ODEs about an equilibrium point $\mathbf{a}_0$, to which the origin of the original coordinate system is shifted.

The resulting flow model is written as

$$\dot{\mathbf{a}}(t) = G\mathbf{a}(t) + B\Gamma(t) \tag{22}$$

where, for the sake of simplicity, the notation $\mathbf{a}(t)$ is maintained for the shifted coordinates. Quadratic stochastic estimation is implemented to correlate real-time measurements of surface pressure fluctuations $p'_j(t)$ at m distinct locations with the modal

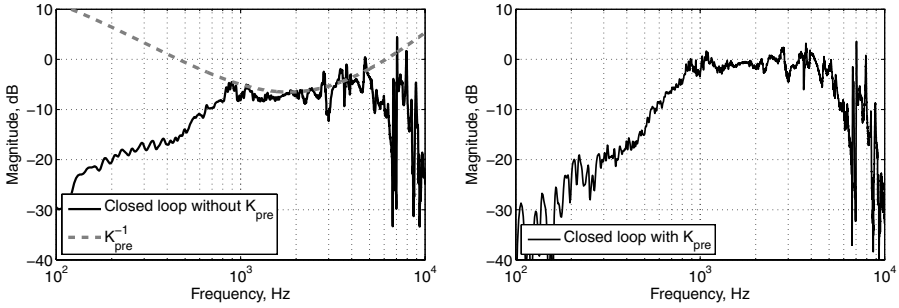

a) Before applying a prefilter **b) After applying a prefilter**

Fig. 10 Frequency response of the compensated actuator system a) without and b) with a prefilter $K_{\text{pre}}(s)$.

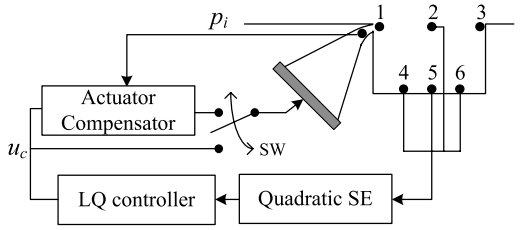

Fig. 11 Schematic of cavity flow control system including the actuator compensator. Pressure transducers 2, 4, 5, and 6 are used for stochastic estimation (SE) of system variables.

coefficients in Eq. (22). The estimates of the modal coefficients are defined as

$$\hat{a}_i(t) = C^{ij} p'_j(t) + D^{ijk} p'_j(t) p'_k(t) \qquad i = 1 \cdots n, \qquad j,k = 1 \cdots m \tag{23}$$

In this study, surface pressure measurements were obtained at four distinct locations ($m = 4$) on the cavity wall, shown schematically in Fig. 11. Further discussions about the stochastic estimation and control input separation can be found in Samimy et al. [13] and Caraballo et al. [39] A feedback controller from the estimated states has been derived in the form

$$\Gamma(t) = -K_{\mathrm{LQ}} \hat{\mathbf{a}}(t) \tag{24}$$

where the gain matrix K_{LQ} has been selected using linear-quadratic control to minimize a quadratic cost function of the system states and the input energy [34]. A representation of the integration of the actuator compensator and the cavity flow control system is depicted in Fig. 11. When the compensator is active, the control signal u_c generated by the cavity flow controller is used as a reference command for the compensator. Otherwise, the signal u_c is directly provided as a voltage signal to the compression driver.

B. Closed-Loop Experimental Results

With the actuator compensator embedded into the cavity flow control system, closed-loop experiments were performed at the baseline Mach 0.3 flow condition. Figure 12 shows sound pressure level (SPL) spectra of the surface pressure acquired by transducer 5 in Fig. 11. In absence of feedback control (baseline flow), the sound pressure level of the flow resonance reaches 135 dB. Engaging the LQ feedback control reduces this peak to a level just below 120 dB in absence of actuator compensation, as shown in Fig. 12a, while several low-magnitude peaks appear in the frequency range 2–7 kHz. When the compensator of the actuator dynamics is enabled, the closed-loop response improves considerably, as shown in Fig. 12b. The peaks labeled A, B, D, and E in Fig. 12a are significantly reduced. Consequently, the maximum peak of the sound pressure levels is reduced below 112 dB for the entire frequency range, while no spurious components exceed the low-frequency noise plateau.

For the same experiment, Fig. 13 compares the spectrum of the actuator output p_i (inside pressure) with that of the reference signal u_c generated by the LQ controller. In Fig. 13a, the peaks a–e in the controller signal and the peaks a′–e′ in the actuator output represent the frequency components corresponding to the peaks A–E in Fig. 12a. Comparing Fig. 13a with the frequency response in Fig. 6 reveals that without compensation the actuator output is strongly dominated by the actuator own dynamics, and the control command is severely distorted. It should be noted that the peaks a (2185 Hz), d (5432 Hz), and e (7062 Hz) are intrinsic to the actuator dynamics, whereas the peaks b (2844 Hz) and c (3198 Hz) are associated with the cavity flow dynamics. In contrast, the compensator forces the actuator output to closely follow the control signal within the frequency range of 1–5 kHz, as shown in Fig. 13b. Furthermore, the frequency components of the actuator output above 5 kHz are effectively attenuated so that those peaks do not appear in the pressure measurements in closed-loop operation. The compensator achieves its goal to suppress the uncertainty caused by the actuator dynamics from the closed-loop response. It allows not only to recover the best possible performance of the LQ cavity flow

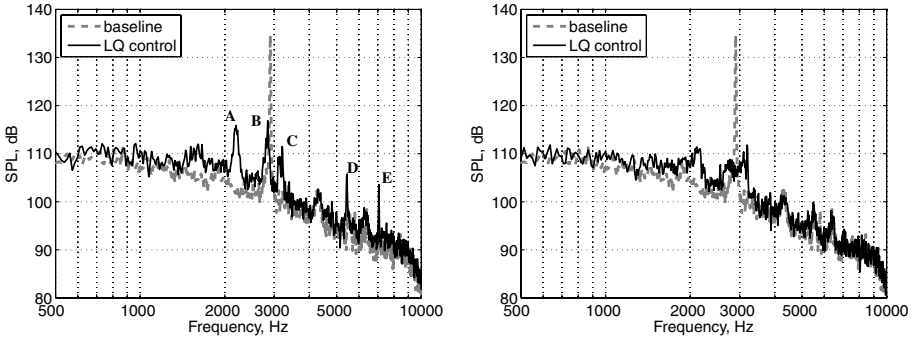

a) Actuator compensation is inactive **b) Actuator compensation is active**

Fig. 12 SPL spectra in closed loop without actuator compensation a), and with actuator compensation b). The freestream Mach number is 0.3.

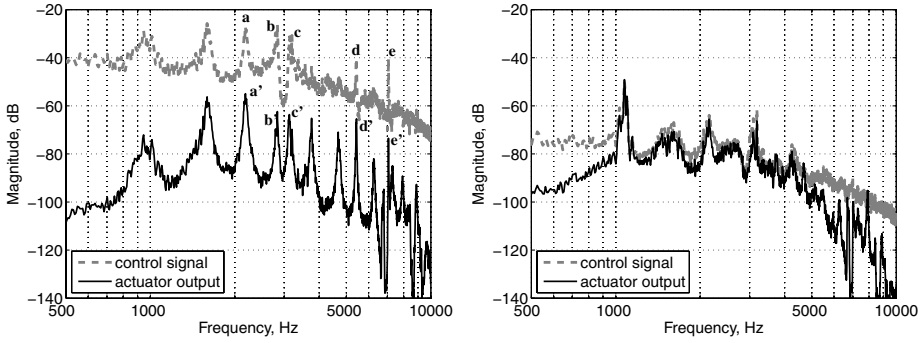

a) Actuator compensation is inactive **b) Actuator compensation is active**

Fig. 13 Spectra of the reference signal of the LQ controller and the actuator output in closed loop without actuator compensation a), and with actuator compensation b). The freestream Mach number is 0.3.

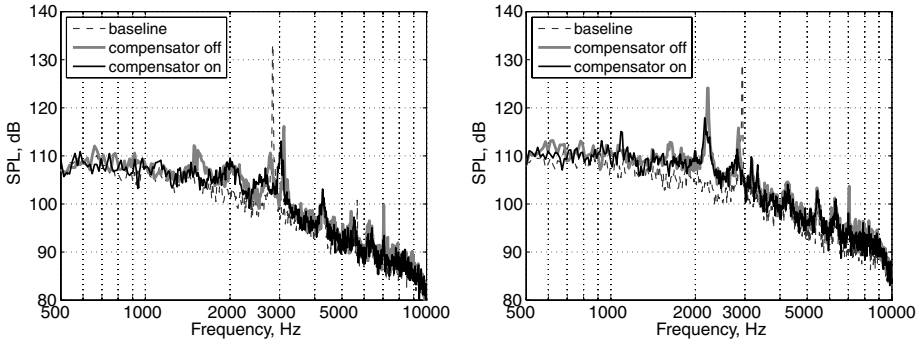

Fig. 14 Closed-loop SPL spectra in off-design conditions. Freestream Mach numbers are 0.28 a) and 0.32 b), respectively.

controller, but also to facilitate the assessment of the overall performance of the control scheme.

The freestream Mach number was varied between 0.28 and 0.32 to explore the effects of the compensator on the performance of the cavity flow control under off-design conditions. Figure 14 presents the SPL spectra of the surface pressures at transducer 5 for Mach 0.28 and 0.32, respectively. In the Mach 0.28 case, the feedback control still benefits from the compensator, which attenuates spurious frequency components compared to the case without compensation. At Mach 0.32, the feedback control without the compensator suppresses the resonance peak at 2930 Hz, while creating the strong peak above 125 dB at 2209 Hz. It implies that the control performance is deteriorated at off-design conditions. Nonetheless, the addition of the compensator effectively decreases the magnitudes of several resonance peaks. These results seem to confirm that the compensator improves the robustness of the original flow control system, thereby extending the range of freestream conditions where the control strategy is effective.

VI. Conclusions

The input–output response of a typical synthetic jetlike compression driver used for cavity flow control exhibits strong intrinsic resonance peaks spread over a wide frequency range, as its dynamics are closely related to infinite-dimensional acoustic dynamics of the actuator. As a necessary step to improve the performance of existing feedback cavity flow control architecture, a servocompensator for the actuator dynamics was designed on the basis of a control-oriented model of the actuator. A subspace-based system identification method was used to develop a model in the form of a time-delay linear system which matches the physical system in the frequency range of interest for feedback cavity flow control experiments. A Smith-predictor-type structure with a 2 degree-of-freedom controller designed minimizing an H_∞ mixed-sensitivity criterion was successfully implemented for the synthesis of the compensator. The actuator compensator is shown to significantly improve the performance of the overall closed-loop flow control system at design conditions, by suppressing undesirable spurious peaks in the sound pressure spectra. Furthermore, experimental results for off-design freestream conditions showed that the compensator allows an extension of the range of Mach numbers where the flow control system is effective, by reducing the model uncertainty in closed loop.

Although the results presented and discussed in this paper concern a specific experimental apparatus, the actuator is representative of a large class of devices used in cavity flow control applications [21]. Consequently, the proposed approach constitutes a methodology of general applicability which presents clear advantages, in terms of scalability and ease of implementation, over a servocompensator design based on first-principle modeling.

Acknowledgments

This work was supported by the U.S. Air Force Research Laboratories/Air Vehicles Directorate (AFRL/VA) and the U.S. Air Force Office of Scientific Research (AFOSR) through the Collaborative Center of Control Science (CCCS) (Contract F33615-01-2-3154). The authors would like to thank their colleagues at CCCS, Hitay Özbay, James Myatt, Coşku Kasnakoğlu, Edgar Caraballo, and Jesse Little for assistance and fruitful discussions.

References

[1] Gharib, M., "Response of the Cavity Shear Layer Oscillations to External Forcing," *AIAA Journal*, Vol. 25, No. 1, 1987, pp. 43–47.

[2] Rowley, C. W., Colonius, T., and Basu, A. J., "On Self-Sustained Oscillations in Two-Dimensional Compressible Flow over Rectangular Cavities," *Journal of Fluid Mechanics*, Vol. 455, April 2002, pp. 315–346.
doi:10.1017/S0022112001007534

[3] Samimy, M., Debiasi, M., Caraballo, E., Malone, J., Little, J., Özbay, H., Efe, M. Ö., Yan, P., Yuan, X., DeBonis, J., Myatt, J. H., and Camphouse, R. C., "Exploring Strategies for Closed-Loop Cavity Flow Control," AIAA Paper 2004-0576, 2004.

[4] Staneck, M., Raman, G., Kibens, V., Ross, J., Odedra, J., and Peto, J., "Control of Cavity Resonance Through Very High Frequency Forcing," AIAA Paper 2000-1905, 2000.

[5] Debiasi, M., and Samimy, M., "Logic-Based Active Control of Subsonic Cavity Flow Resonance," *AIAA Journal*, Vol. 42, No. 9, 2004, pp. 1901–1909.

[6] Cattafesta, L. N., Williams, D. R., Rowley, C. W., and Alvi, F. S., "Review of Active Control of Flow-Induced Cavity Resonance," AIAA Paper 2003-3567, 2003.

[7] Rowley, C., and Williams, D. R., "Dynamics and Control of High-Reynolds-Number Flow over Open Cavities," *Annual Review of Fluid Mechanics*, Vol. 38, Jan. 2006, pp. 251–276.
doi:10.1146/annurev.fluid.38.050304.092057

[8] Rowley, C. W., Williams, D. R., Colonius, T., Murray, R. M., and MacMynowski, D. G., "Linear Models for Control of Cavity Flow Oscillations," *Journal of Fluid Mechanics*, Vol. 547, Jan. 2006, pp. 317–330.
doi:10.1017/S0022112005007299

[9] Yan, P., Debiasi, M., Yuan, X., Little, J., Özbay, H., and Samimy, M., "Experimental Study of Linear Closed-Loop Control of Subsonic Cavity Flow," *AIAA Journal*, Vol. 44, No. 5, 2006, pp. 929–938.

[10] Efe, M. Ö., Debiasi, M., Yan, P., Özbay, H., and Samimy, M., "Control of Subsonic Cavity Flows by Neural Networks—Analytical Models and Experimental Validation," AIAA Paper 2005-0294, 2005.

[11] Caraballo, E., Yuan, X., Little, J., Debiasi, M., Yan, P., Serrani, A., Myatt, J. H., and Samimy, M., "Feedback Control of Cavity Flow Using Experimental Based Reduced Order Model," AIAA Paper 2005-5269, 2005.

[12] Caraballo, E., Yuan, X., Little, J., Debiasi, M., Serrani, A., Myatt, J. H., and Samimy, M., "Further Development of Feedback Control of Cavity Flow Using Experimental Based Reduced Order Model," AIAA Paper 2006-1405, 2006.

[13] Samimy, M., Debiasi, M., Caraballo, E., Serrani, A., Yuan, X., Little, J., and Myatt, J. H., "Feedback Control of Subsonic Cavity Flows Using Reduced-Order Models," *Journal of Fluid Mechanics*, Vol. 579, May 2007, pp. 315–346.
doi:10.1017/S0022112007005204

[14] Skogestad, S., and Postlethwaite, I., *Multivariable Feedback Control*, 2nd ed., Wiley, West Sussex, England, U.K., 2005.

[15] Rathnasingham, R., and Breuer, K. S., "Coupled Fluid-Structural Characteristics of Actuators for Flow Control," *AIAA Journal*, Vol. 35, No. 5, 1997, pp. 832–837.
[16] Sharma, R. N., "An Analytical Model for Synthetic Jet Actuation," AIAA Paper 2006-3035, 2006.
[17] Gallas, Q., Holman, R., Nishida, T., Carroll, B., Sheplak, M., and Cattafesta, L., "Lumped Element Modeling of Piezoelectric-Driven Synthetic Jet Actuators," *AIAA Journal*, Vol. 41, No. 2, 2003, pp. 240–247.
[18] Ukpai, U. I., and Rediniotis, O., "Dynamic Modeling of a Synthetic Jet Actuator for Hingeless Flow Control," *Proceedings of the 2003 American Control Conference*, IEEE, Piscataway, NJ, 2003, pp. 1704–1709.
[19] Venugopal, R., and Bernstein, D. S., "State Space Modeling of an Acoustic Duct with an End-Mounted Speaker," *Journal of Vibration and Acoustics*, Vol. 120, No. 3, July 1998, pp. 770–775.
[20] Pota, H. R., and Kelkar, A., "Modeling and Control of Acoustic Ducts," *Journal of Vibration and Acoustics*, Vol. 123, No. 1, Jan. 2001, pp. 2–10.
doi:10.1115/1.1311793
[21] Rowley, C. W., Juttijudata, V., and Williams, D. R., "Cavity Flow Control Simulations and Experiments," AIAA Paper 2005-0292, 2005.
[22] Schultz, R. R., "Modeling and Identification of an Acoustic Actuator for Cavity Flow Control," Master's Thesis, The Ohio State University, Columbus, OH, 2006.
[23] McKelvey, T., Fleming, A., and Moheimani, S. O. R., "Subspace-Based System Identification for an Acoustic Enclosure," *Journal of Vibration and Acoustics*, Vol. 124, No. 3, July 2002, pp. 414–419.
doi:10.1115/1.1467653
[24] Chang, C.-Y., and Shyu, K.-K., "A Self-Tuning Fuzzy Filtered-U Algorithm for the Application of Active Noise Cancellation," *IEEE Transactions on Circuits and Systems—I: Fundamental Theory and Applications*, Vol. 49, No. 9, 2002, pp. 1325–1333.
doi:10.1109/TCSI.2002.802350
[25] Wu, J.-D., and Lee, T.-H., "Application of H-Infinity Hybrid Active Controller for Acoustic Duct Noise Cancellation," *International Journal of Vehicle Noise and Vibration*, Vol. 1, Nos. 3–4, 2005, pp. 183–193.
doi:10.1504/IJVNV.2005.007522
[26] Hong, J., Akers, J. C., Venugopal, R., Lee, M.-N., Sparks, A. G., Washabaugh, P. D., and Bernstein, D. S., "Modeling, Identification, and Feedback Control of Noise in an Acoustic Duct," *IEEE Transactions on Control Systems Technology*, Vol. 4, No. 3, 1996, pp. 283–291.
doi:10.1109/87.491202
[27] O'Brien, R. T., Watkins, J. M., Piper, G. E., and Baumann, D. C., "H_∞ Active Noise Control of Fan Noise in an Acoustic Duct," *Proceedings of the American Control Conference 2000*, IEEE, Piscataway, NJ, June 2000, pp. 3028–3032.
[28] Venugopal, R., and Bernstein, D. S., "Adaptive Disturbance Rejection Using ARMARKOV/Toeplitz Models," *IEEE Transactions on Control Systems Technology*, Vol. 8, No. 2, 2000, pp. 257–269.
doi:10.1109/87.826797
[29] Smith, O. J. M., "Closer Control of Loops with Deadtime," *Chemical Engineering Progress*, Vol. 53, No. 5, 1957, pp. 217–219.
[30] McKelvey, T., Akcay, H., and Ljung, L., "Subspace-Based Multivariable System Identification from Frequency-Response Data," *IEEE Transactions on Automatic Control*, Vol. 41, No. 7, 1996, pp. 960–979.
doi:10.1109/9.508900
[31] Ljung, L., *System Identification: Theory for the User*, 2nd ed., Prentice–Hall, Upper Saddle River, NJ, 1998.
[32] Ljung, L., *System Identification Toolbox User's Guide*, The MathWorks, Natick, MA, 2005.
[33] Antoulas, A. C., *Approximation of Large-Scale Dynamical Systems*, Advances in Design and Control, Society for Industrial and Applied Mathematic, Philadelphia, PA, 2005.
[34] Goodwin, G. C., Graebe, S. F., and Salgado, M. E., *Control System Design*, Prentice–Hall, Upper Saddle River, NJ, 2001.
[35] Hoyle, D. J., Hyde, R. A., and Limebeer, D. J. N., "An H_∞ Approach to Two Degree of Freedom Design," *Proceedings of the 30th Conference on Decision and Control*, IEEE, New York, Dec. 1991, pp. 1581–1585.
[36] Balas, G., Chiang, R., Packard, A., and Safonov, M., *Robust Control Toolbox User's Guide*, MathWorks, Natick, MA, 2005.
[37] Glover, K., and Doyle, J., "State-Space Formulae for All Stabilizing Controllers that Satisfy H_∞ Norm Bound and Relations to Risk Sensitivity," *Systems and Control Letters*, Vol. 11, No. 3, Sept. 1988, pp. 167–172.
doi:10.1016/0167-6911(88)90055-2
[38] Efe, M. Ö., and Özbay, H., "Low Dimensional Modeling and Dirichlét Boundary Controller Design for Burgers Equation," *International Journal of Control*, Vol. 77, No. 10, 2004, pp. 895–906.
doi:10.1080/00207170412331270532
[39] Caraballo, E., Little, J., Debiasi, M., Serrani, A., and Samimy, M., "Reduced Order Model for Feedback Control of Cavity Flow—The Effects of Control Input Separation," AIAA Paper 2007-1125, 2007.

N. Chokani
Associate Editor